AERONOMICA ACTA

A - N° 194 - 1978

A dynamical effect in the ionospheric F$_1$ layer

by

C. TAIEB, G. SCIALOM and G. KOCKARTS

FOREWORD

The paper entitled "A dynamical effect in the ionospheric F_1 layer" will be published in Planetary and Space Science. **26**, 1978.

AVANT-PROPOS

L'article intitulé "A dynamical effect in the ionospheric F_1 layer" sera publié dans Planetary and Space Science, **26**, 1978.

VOORWOORD

Het artikel "A dynamical effect in the ionospheric F_1 layer" zal verschijnen in Planetary and Space Science. **26**, 1978.

VORWORT

Die Arbeit "A dynamical effect in the ionospheric F_1 layer" wird in Planetary and Space Science. **26**, 1978 herausgegeben werden.

A DYNAMICAL EFFECT IN THE IONOSPHERIC F_1 LAYER

by

C. TAIEB*, G. SCIALOM* and G. KOCKARTS**

* CRPE, 38 rue du Général Leclerc, F-92131 Issy-les-Moulineaux, France
** IAS, 3 Avenue Circulaire, B-1180 Bruxelles, Belgium

Abstract

Incoherent scatter observations of the ionospheric F_1 layer above Saint-Santin(44.6°N) are analyzed after correction of a systematic error at 165 km and 180 km altitude. The daytime valley observed around 200 km during summer for low solar activity conditions is explained in terms of a downward ionization drift which reaches - 30 m s⁻¹ around 180 km. Experimental determinations of the ion drift confirm the theoretical characteristics required for the summer daytime valley as well as for the winter behaviour without a valley. The computations require an effective dissociative recombination rate of 2.3×10^{-7} $(300/T_e)^{0.7}$ ($cm^3 s^{-1}$) and ionizing fluxes compatible with solar activity conditions at the time when the valley is observed.

Résumé

Des observations par diffusion incohérente dans la région ionosphérique F_1 au-dessus de Saint-Santin (44.6°N) ont été analysées après correction d'une erreur systématique à 165 km et à 180 km d'altitude. Aux environs de 200 km, la vallée diurne, observée durant l'été pour des conditions de faible activité solaire, est expliquée par un transport des particules ionisées vers le bas atteignant une vitesse de - 30 m s⁻¹ vers 180 km. Des déterminations expérimentales de la vitesse ionique confirment les caractéristiques des profils théoriques requis pour expliquer la vallée diurne en été et l'absence de vallée en hiver. L'accord entre les calculs et les observations exige simultanément un coefficient effectif de recombinaison dissociative de 2.3×10^{-7} $(300/T_e)^{0.7}$ (cm^3 s^{-1}) et un flux solaire ionisant compatible avec les conditions d'activité solaire existant lors de l'observation de la vallée.

Samenvatting

Waarnemingen van incoherente verstrooiing op de F_1-laag, onderscheidelijk op een hoogte van 165 km en 180 km, boven Saint-Santin (44,6°N) werden ontleed na voorafgaandelijk ontdaan te zijn van een systematische fout. De trog die 's zomers overdag ontstaat op 200 km bij een geringe werkingsgraad van de zon wordt verklaard door een dalende beweging van geïoniseerde bestanddelen die op 180 km hoogte een snelheid hebben van - 30 m s⁻¹. Proefondervindelijke waarden van de ionensnelheden stemmen goed overeen met de kenmerken der theoretische profielen die vereist zijn om 's zomers het bestaan van een trog overdag te verklaren evenals de verschijnselen in de winter wanneer er geen trog is. De berekeningen vergen een daadwerkelijke dissociatieve recombinatie constante van 2.3×10^{-7} $(300/T_e)^{0.7}$ cm³ s⁻¹, rekening houdende met een ioniserende stralingsflux die overeenstemt met de werkingsgraad van de zon op het ogenblik dat de trog werd waargenomen.

Zusammenfassung

Inkohärente Streuungsbeobachtungen der ionosphärischen F_1 Schichte über Saint-Santin (44.6°N) werden nach Verbesserung eines systematischen Fehlers auf 165 km und 180 km Höhe analisiert. Im Sommer und für schwacher Sonnenaktivität wird das tägliche beobachtete Tal in der Umgebung von 200 km erklärt mit Hilfe einer herunterwärts Ionisationsdriftgeschwindigkeit die etwa - 30 m s⁻¹ auf 180 Höhe erreicht. Messungen der Ionisationsdriftgeschwindigkeit bestätigen der theoretische Charakteristiken, die für das tägliche Sommertal und für das Winterbetragen ohne Tal nötig sind. Die Rechnungen erfordern einen effektiven Trennungsrekombinationskoeffizient von 2.3×10^{-7} $(300/T_e)^{0.7}$ (cm³ s⁻¹) und eine Ionisationsstrahlung, die mit dem Sonnenaktivitätszustand, wenn das Tal beobachtet ist, übereinstimmt.

1. INTRODUCTION

The F_1 layer of the terrestrial ionosphere is generally regarded as being well described by photochemical processes (see Rishbeth and Garriott, 1969; Banks and Kockarts, 1973) and transport phenomena are usually not important during the day (Schunk and Walker, 1973). Photochemistry alone can lead to a daytime F_1 *ledge* discovered by Appleton (1933) but not to a daytime F_1 *valley* which is observed above Saint-Santin (44.63° N, 02.22° E geographic coordinates). The purpose of the present paper is to provide an explanation of such a daytime irregularity (Taieb *et al.*, 1975) by using an ionic wind effect confirmed by observations at the French multistatic incoherent scatter facility.

The irregularity is characterized by a daytime valley in the electron density profile of the F_1 layer. Instead of observing a continuous increase of the electron density above 120 km, it appears that the concentration increases up to a value n_{MAX} at height z_{MAX}, then it decreases to a value n_{MIN} at altitude z_{MIN}, and finally starts to increase again towards the normal F_2 peak value. Incoherent scatter observations between 1967 and 1972 were analyzed by Taieb *et al.* (1975) who showed that the phenomenon is seasonal and solar activity dependent with an important diurnal variation. The importance of the phenomenon was characterized by a valley parameter $\delta = 100 \times (n_{MAX} - n_{MIN})/n_{MAX}$. The formation of the valley starts several hours after sunrise between 07.00 and 10.00 UT. The valley parameter δ reaches its maximum value around noon, decreases in the afternoon and disappears between 14.00 and 18.00 UT. The valley is only present from March to the beginning of September. During the rest of the year one observes the normal behaviour of the F_1 layer without this valley. Finally, there is no valley, even between March and September, for high solar activity conditions, i.e. from 1967 to 1969 in the data presently analyzed.

The morphology of the phenomenon described by Taieb *et al.* (1975) qualitatively remains valid although a numerical error has been recently detected in the general computer program used for the reduction of the data gathered since 1971 with the French incoherent scatter facility. Before the correction of this error in 1977, electron densities determined after 1971 were systematically underestimated at two altitudes, namely 165 km and

180 km. Although this correction unfortunately falls in the height range analyzed by Taieb *et al.* (1975) it does not affect the existence of the daytime valley phenomenon with its diurnal, seasonal and solar activity variations. Two quantitative consequences, however, result from this correction :

- the valley parameter δ is between 5% and 10% instead of 10% and 25%;
- the density maximum occurs near 180 km (instead of 150 km) and the density minimum is around 200 km (instead of 165 km).

Fig. 1 shows a comparison between the density profiles before (Taieb *et al.*, 1975) (dashed line) and after (full line) the correction for August 9, 1972 at 10.30 UT.

The corrected electron density profiles will be analyzed by using the electron conti-nuity equation in which a realistic transport effect will be included in order to reproduce reasonably well the observed concentrations. Winter and summer conditions will be examined separately since the dynamical behaviour is completely different. The theoretical ionic movements required to explain the phenomena will be compared with observations made with the French multistatic incoherent scatter facility. Such a comparison will show that the theoretical ionic wind is compatible with the ionic drift observed at Saint-Santin.

2. PHOTOCHEMICAL EQUILIBRIUM

Since the time constants necessary to reach photochemical equilibrium conditions are usually less than 10 s in the E region and less than 1.000 s in the F_1 region (see Banks and Kockarts, 1973), a first attempt to explain the daytime F_1 layer was made by considering the classical balance between ionic production and loss. Such an approach requires the knowledge of a neutral atmospheric model in which ionic production by solar ultraviolet radiation and by ion-neutral reactions can be equated to ionic loss by ion-neutral reactions and by ion-electron dissociative recombination. With the usual assumption of electric charge neutrality it is then possible to compute the electron concentration by solving a system of algebraic equations.
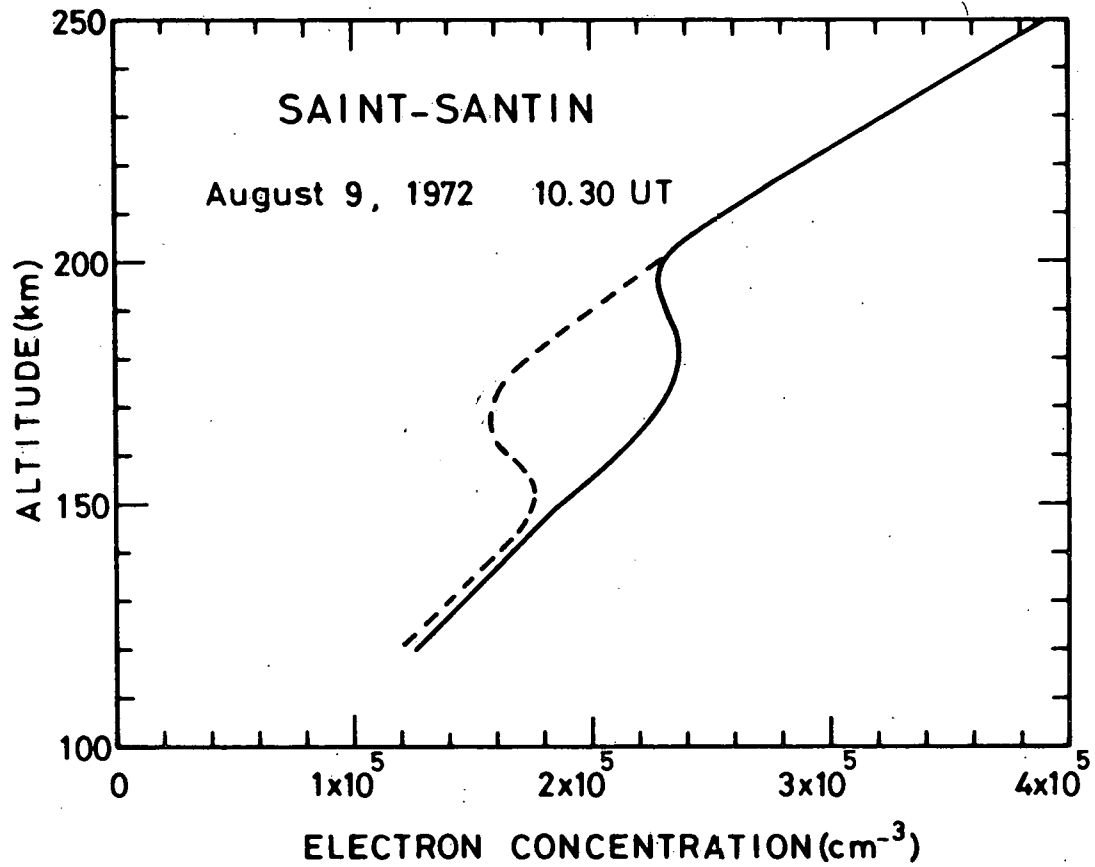
Fig. 1.- Electron density profile above Saint-Santin on August 9, 1972 at 10.30 UT. Full curve is obtained after correction of the systematic error detected in 1977. Dashed curve corresponds to the uncorrected profile.

The vertical temperature distribution $T(z)$ is given by (Bates, 1959)

$$T(z) = T_\infty - (T_\infty - T_{120}) e^{-s(z - 120)} \tag{1}$$

where z is the altitude in km, T_∞ is the thermopause temperature, T_{120} is the temperature at the lower boundary and s is a slope parameter. The last three quantities can be deduced from incoherent scatter measurements. We adopt $T_\infty = 1100$ K, $T_{120} = 400$ K and $s = 0.026$ km^{-1} in a set of computations when the neutral concentrations at 120 km arbitrarily vary within the following limits :

$$5 \times 10^9 \;\; cm^{-3} \leqslant n(O) \leqslant 5 \times 10^{11} \; cm^{-3}$$

$$1 \times 10^9 \;\; cm^{-3} \leqslant n(O_2) \leqslant 4 \times 10^{10} \; cm^{-3}$$

$$1 \times 10^{11} \; cm^{-3} \leqslant n(N_2) \leqslant 4 \times 10^{11} \; cm^{-3}$$

Such extreme variations of the neutral concentrations at 120 km are highly improbable, but they were used to see if photochemical equilibrium could eventually explain the daytime ionospheric valley.

The solar ultraviolet fluxes (Hinteregger, 1976; Schmidtke, 1976) as well as the absorption and ionization cross sections adapted from Banks and Kockarts (1973) are given in Table I. In the altitude range of interest (120 - 250 km) the important chemical reactions are :
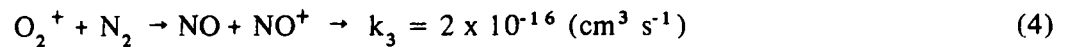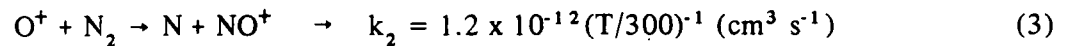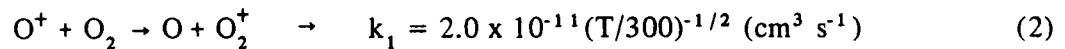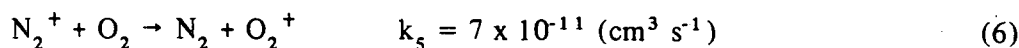
$$O^+ + O_2 \rightarrow O + O_2^+ \quad \rightarrow \quad k_1 = 2.0 \times 10^{-11} (T/300)^{-1/2} \; (cm^3 \; s^{-1}) \tag{2}$$

$$O^+ + N_2 \rightarrow N + NO^+ \quad \rightarrow \quad k_2 = 1.2 \times 10^{-12} (T/300)^{-1} \; (cm^3 \; s^{-1}) \tag{3}$$

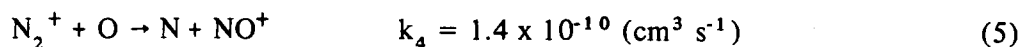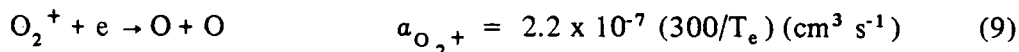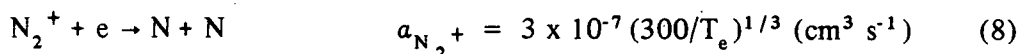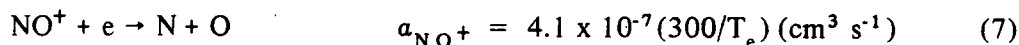$$O_2^+ + N_2 \rightarrow NO + NO^+ \rightarrow k_3 = 2 \times 10^{-16} \; (cm^3 \; s^{-1}) \tag{4}$$

TABLE I : Solar ultraviolet fluxes (10^9 photons $cm^{-2} s^{-1}$), absorption (A) and ionization (I) cross sections ($10^{-18} cm^2$)

Wavelength (nm)	Flux (Hinteregger, 1976)	Flux (Schmidtke, 1976)	Cross sections				
			O	O_2		N_2	
			A = I	A	I	A	I
102.7 - 91.1	9.1	13.4	–	4.8	3.3	0.1	–
91.1 - 80.0	8.6	11.7	3.0	15.0	5.7	5.0	–
80.0 - 70.0	2.1	2.9	4.0	21.8	11.1	26.5	18.0
70.0 - 63.0	0.2	0.3	8.0	22.3	22.3	24.4	23.5
63.0 - 46.0	6.0	8.7	10.0	25.6	24.8	24.0	23.5
46.0 - 37.0	0.5	0.7	9.0	19.3	19.3	22.4	22.4
37.0 - 28.0	11.7	15.0	7.0	16.6	16.6	12.1	12.1
28.0 - 20.5	3.6	6.7	5.0	13.0	13.0	11.0	11.0
20.5 - 16.5	3.6	7.3	3.3	6.6	6.6	2.1	2.1
16.5 - 15.0	0.4	1.2	0.9	1.8	1.8	0.7	0.7

$$N_2^+ + O \rightarrow N + NO^+ \qquad k_4 = 1.4 \times 10^{-10} \ (cm^3 \ s^{-1}) \qquad (5)$$

$$N_2^+ + O_2 \rightarrow N_2 + O_2^+ \qquad k_5 = 7 \times 10^{-11} \ (cm^3 \ s^{-1}) \qquad (6)$$

with the dissociative recombination processes

$$NO^+ + e \rightarrow N + O \qquad a_{NO^+} = 4.1 \times 10^{-7}(300/T_e) \ (cm^3 \ s^{-1}) \qquad (7)$$

$$N_2^+ + e \rightarrow N + N \qquad a_{N_2^+} = 3 \times 10^{-7} (300/T_e)^{1/3} \ (cm^3 \ s^{-1}) \qquad (8)$$

$$O_2^+ + e \rightarrow O + O \qquad a_{O_2^+} = 2.2 \times 10^{-7} \ (300/T_e) \ (cm^3 \ s^{-1}) \qquad (9)$$

The reaction rate coefficients are taken from the compilation of Banks and Kockarts (1973). It is also possible to determine some important ionospheric reaction rates from the Atmosphere Explorer *in situ* measurements. The results obtained by Torr *et al.* (1977a) for k_2 and by Torr *et al.* (1977b) for k_4 are in good agreement with the values used in the present computations. The dissociative recombination rates a_{NO^+} and $a_{O_2^+}$ also agree fairly well with the laboratory measurements of Walls and Dunn (1974).

Allowing extreme variations of the lower boundary conditions and using the previously described photochemical scheme it is impossible to obtain a daytime valley in the F_1 region even by changing arbitrarily the dissociative recombination rates by a factor of two. At best a ledge could be obtained.

A last attempt has been made by introducing the effect of neutral nitric oxide through the reaction

$$NO + O_2^+ \rightarrow O_2 + NO^+ \qquad (10)$$

with a rate coefficient $k_6 = 4.4 \times 10^{-10} \ cm^3 \ s^{-1}$ (Lindinger *et al.*, 1975). A set of arbitrary nitric oxide profiles was used and only *negative* values of NO could lead to valley. Such an

unrealistic assumption of course must be eliminated and it appears that photochemical equilibrium cannot explain the observed valley. It is, therefore, necessary to include a transport effect in a realistic analysis.

3. TRANSPORT EFFECT DURING SUMMER

The continuity equation for electrons assuming a horizontal stratification of the ionosphere can be written under steady state conditions in the F_1 layer as

$$\frac{\partial}{\partial z}\left[n_e v_e\right] = P_e - \left[a_{NO^+}n(NO^+) + a_{N_2^+}(N_2^+) + a_{O_2^+}n(O_2^+)\right]n_e \tag{11}$$

where n_e is the electron concentration, v_e is the vertical electron velocity and P_e is the electron production rate by photoionization. The loss term results from processes (7) to (9). Introducing the composition parameter $p = n(O^+)/n_e$ and the effective recombination coefficient

$$a = \frac{a_{NO^+}n(NO^+) + a_{N_2^+}n(N_2+) + a_{O_2^+}n(O_2^+)}{n(NO^+) + n(N_2^+) + n(O_2^+)} \tag{12}$$

equation (11) becomes

$$\frac{\partial}{\partial z}[n_e v_e] = P_e - a(1 - p)n_e^2 \tag{13}$$

with

$$n_e = n(O^+) + n(NO^+) + n(N_2^+) + n(O_2^+) \tag{14}$$

The electron continuity equation (13) can be used to determine which electron velocity profile v_e is compatible with the observed daytime valley. Such a vertical velocity profile must then be compared with the velocity profile measured by incoherent scatter sounding at the same time as the electron density profile. Furthermore, a relationship must be established between the permanent character of the observed phenomena (i.e. the systematic presence of the valley during several months of the year) and the ion or electron velocity resulting from neutral circulation and ionospheric electric fields. Such an analysis takes into account the various photochemical parameters (solar fluxes, dissociative recombination rates, composition parameter) whose influence can be pointed out. Summer conditions for low solar activity will be examined first and the winter situation without a valley will be discussed in section 4.

3.1. Ion velocity model

When the electron density is assumed to be known, it is possible to deduce the electron or average ion vertical velocity profile by solving Equation (13) for a specific set of photochemical parameters. Compatibility with the presence of a daytime valley is assured if the velocity v_e has following characteristics :

- v_e must be almost zero at low altitude near 130 km;
- above 130 km altitude v_e must be negative (i.e. downwards) and it must reach a value of the order of - 25 to - 30 m s^{-1} near 180 km altitude;
- the velocity gradient must change its sign above that height and v_e must tend towards zero or a positive value around 220 km altitude.

The full curve on Fig. 2 represents a typical profile obtained on May 6, 1975 at 11.00 UT. Solar fluxes measured by Hinteregger (1976) for low solar activity conditions have been used with the absorption and ionization cross sections given in Table 1. Since the vertical electron profile is obtained in approximately one hour, an average zenith angle χ of 33° (sec χ = 1.19) is adopted at Saint-Santin on May 6, 1975 at 11.00 UT. Neutral concentrations n(X) are computed from the relation
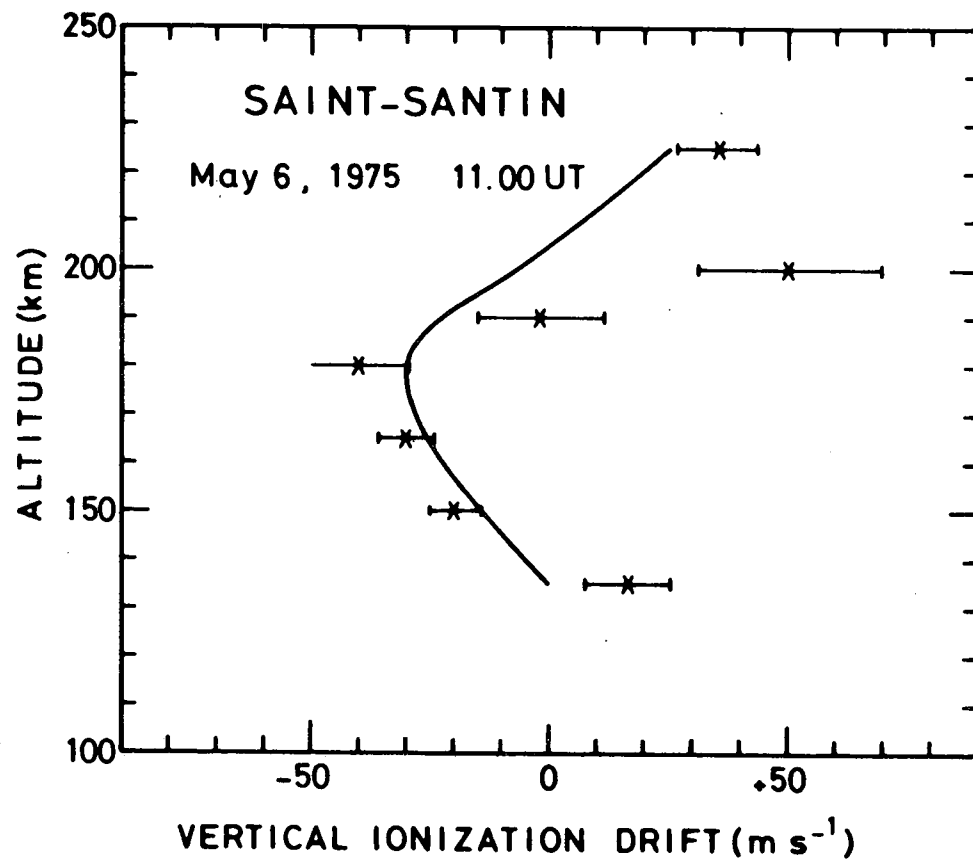
Fig. 2.- Vertical ionization drift (full curve) resulting from the electron continuity equation. Crosses represent velocities with their error bars observed on May 6, 1975 between 10.00 and 11.00 UT at various altitudes.

$$n(X) = n_{120}(X) [T_{120}/T(z)] \exp - \int_{120}^{z} \frac{dz}{H_x} \tag{15}$$

with the temperature profile (1) in which $T_\infty = 1100$ K, $T_{120} = 400$ K and $s = 0.026$ km^{-1} were obtained from the incoherent scatter sounding on May 6, 1975 (Carru et al., 1967; Bauer et al., 1970), H_x is the partial pressure scale height for each neutral constituent X. The concentrations at 120 km are respectively, $n(O) = 4 \times 10^{10}$ cm^{-3}, $n(O_2) = 3 \times 10^{10}$ cm^{-3} and $n(N_2) = 2.8 \times 10^{11}$ cm^{-3} (Mayr et al., 1976). The effective dissociative recombination a is adopted as

$$a = 2.3 \times 10^{-7} (300/T_e)^{0.7} \ (cm^3 \ s^{-1}) \tag{16}$$

and the effect of this expression will be discussed later. The height variation of the composition parameter p is given by Oliver (1975)

$$p = 2/\left\{ 1 + \left[1 + 8 \times \exp\left(\frac{z_{50} - z}{H} \right) \right]^{1/2} \right\} \tag{17}$$

where z_{50} is the altitude for which $p = 0.5$ and H is an empirical scale height. Incoherent scatter measurements lead to $z_{50} = 190$ km and $H = 20$ km for summer conditions.

With the empirical velocity profile of Fig. 2, equation (13) is solved for the electron density. Fig. 3 shows satisfactory agreement between empirical and observed profiles. This implies that the characteristics of the velocity profile given on Fig. 2 are realistic. Some variations are, however possible. The valley depth becomes larger when the absolute value of the minimum velocity increases. Furthermore, variations in the altitude of the velocity minimum imply variations of the altitude of the electron density maximum. The density maximum around 180 km altitude actually results from a downward electron flux coming from higher levels and reaching a value of 6-8 $\times$ 10^8 electrons cm^{-2} s^{-1} around 180 km.

The agreement between the empirical and observed profiles of Fig. 3 must, however, be sustained by observations of the ion drift which up to now has been adjusted in a way to
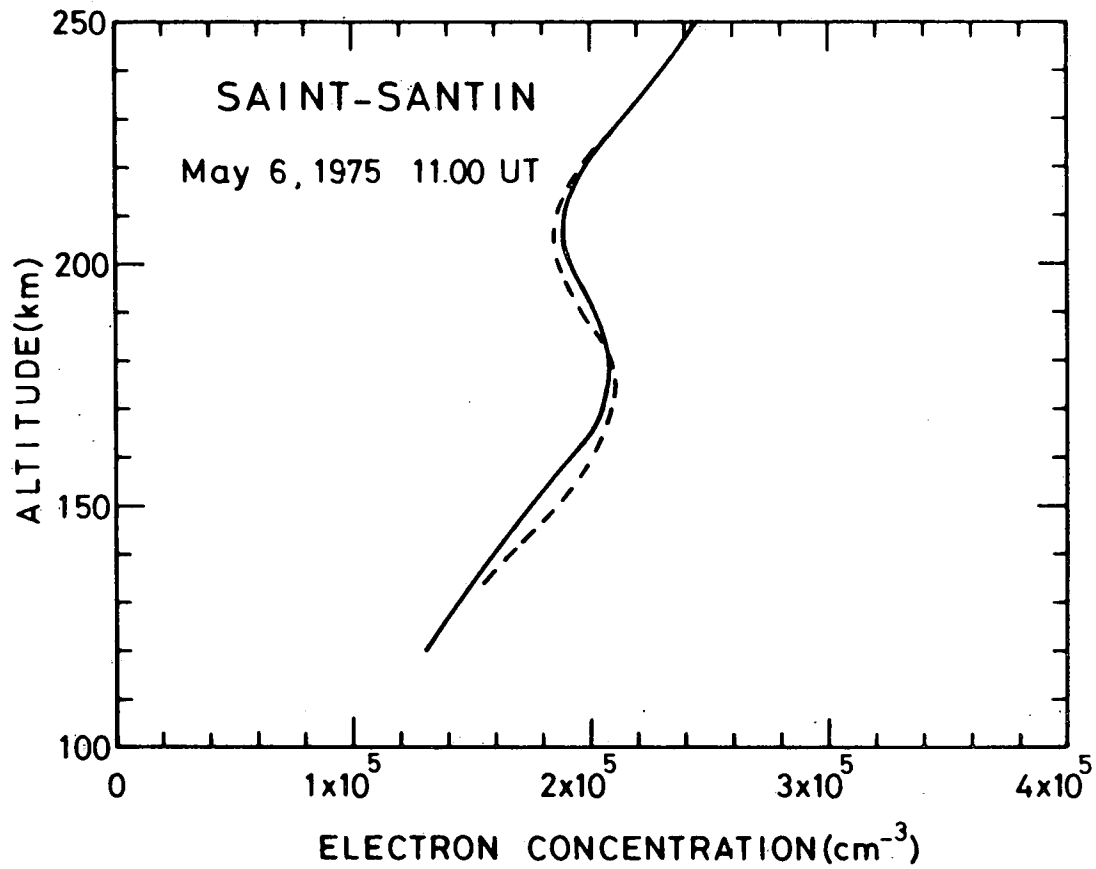
Fig. 3.- Comparison between observed electron density profile (full curve) on May 6, 1975 at 11.00 UT and computed profile (dashed curve) obtained with the empirical ionization drift of Fig. 2.

reproduce the observed electron density profile. The French multistatic incoherent scatter facility (Bauer *et al.*, 1974) fortunately allows a determination of three components of the ion drift vector (Blanc *et al.*, 1977) Fig. 2 also shows the observed vertical ion drift deduced on May 6, 1975 from measurements at three receiving stations. At a given time, the ion drift is measured along the bisector of the emitted and received beams. The altitude of the measured component is not the same for each station. Homogeneous data are obtained at a given height by averaging over a two hours period with running means over 30 min time steps. Height interpolation leads to the ion drift vector in the reference frame of the three stations. A change of coordinates gives the vertical ion drift shown on Fig. 2. Observed values of Fig. 2 clearly indicate a minimum in the vertical velocity of the order of -40 m s^{-1} around 180 km. The observed values of Fig. 2 are in satisfactory agreement with the postulated profile despite of the rather poor time resolution of the measurements. The adopted ion velocity model is, therefore, confirmed by observations. It must, however, be realized that each ionic species has its own velocity. We consider here an average ion velocity since this quantity is accessible through the incoherent scatter data.

3.2. Ion drift effect on the permanence of the daytime valley

Although the observations of May 6, 1975 are compatible with the ion drift of Fig. 2, one has to explain the permanence of the F_1 region valley during low solar activity summer conditions. When ion diffusion is neglected, it is possible to show (Amayenc, 1975) that the ion drift component $\vec{v}_{i\perp}$ perpendicular to the magnetic field $\vec{B}$ is given by

$$\vec{v}_{i\perp} = \vec{v}_{n\perp}\,\frac{r_i^2}{1+r_i^2} + \frac{\vec{v}_{n\perp} \times \vec{B}}{B}\,\frac{r_i}{1+r_i^2} + \frac{\vec{E}_\perp}{B}\,\frac{r_i}{1+r_i^2} + \frac{\vec{E}_\perp \times \vec{B}}{B^2}\,\frac{1}{1+r_i^2} \tag{18}$$

where $\vec{v}_{n\perp}$ is the neutral wind velocity vector perpendicular to $\vec{B}$, $\vec{E}_\perp$ is the electric field vector perpendicular to $\vec{B}$ and r_i is the ratio of the mean ion-neutral collision frequency ν_{in} to the mean ion gyrogrequency ω_i.

Knowledge of the various parameters in Equation (18) leads to the two components v_{ix} and v_{iy} of $\vec{v}_i$. The third component $v_{i\parallel}$ parallel to the magnetic field can be identified with the

neutral wind component parallel to $\vec{B}$ when ion diffusion is neglected below 200 km altitude. Once the three components v_{ix}, v_{iy} and $v_{i\parallel}$ are known in the geomagnetic reference frame, a coordinate transformation leads to the vertical component v_{iz} in the geographical reference frame. A brief description of the quantities involved in Equation (18) will be given before showing numerical results.

Using the ion-neutral collision frequencies given by Stubbe (1968), it is possible to write the mean ion-neutral collision frequency as a function of the composition parameter p and of the neutral concentrations in the following form

$$\nu_{in} = \frac{1 \times 10^{-15} p}{2 - p} [0.93(T/1000)^{0.37} n(O) + 0.687 n(N_2) + 0.667 n(O_2)]$$

$$+ \frac{2 \times 10^{-15} (1 - p)}{2 - p} [0.25 n(O) + 0.415 n(N_2) + 0.585(T/1000)^{0.18} n(O_2)] \quad (19)$$

where T is the neutral gas temperature. Expression (19) is obtained by using the same atomic mass for NO^+ and O_2^+ (i.e. 32 amu).

The mean gyrofrequency is given by

$$\omega_i = p \, \omega(O^+) + (1 - p) \, \omega(O_2^+) \quad (20)$$

where the mass of NO^+ has also been assumed to be the mass of O_2^+.

The adopted neutral wind model is the analytical model developped by Amayenc (1974) from incoherent scatter measurements of v_{in}. The north- south component of the neutral wind is considered in this model as resulting from a 24 hour diurnal tide and a 12 hour semidiurnal tide for which phases and amplitudes are determined. The east-west component is deduced from the north- south component by a phase change of $\pi/2$.

The electric field $\vec{E}_\perp$ is deduced from drift measurements obtained by incoherent scatter measurements during five days in July between 1973 and 1975 for low solar activity conditions. Since it takes 30 to 45 min to obtain a vertical ion drift profile between 120 km and 200 km, the velocities at each altitude are averaged over one hour time interval and a diurnal variation of $\vec{E}_\perp$ is deduced from running means over 30 minute interval (Blanc and Amayenc, 1976).

Using relation (14) and the procedure which has been described, one obtains the vertical ion profiles of Fig. 4 at 09.00 and 10.00 UT for three hypotheses about the electric field : i.e. zero electric field, electric field deduced from ionic drift measurements, and electric field with a predominant east-west component. Fig. 4 indicates that the shape and the magnitude of the velocity profile is compatible with the results of Fig. 3. Furthermore, it appears that the electric field at Saint- Santin latitude has no major effect on the shape of the velocity profile. The absolue value of the ion drift, however, depends on the electric field when the east-west component (-2mV/m) in particular is predominant. In the present case an east-west component of -0.2mV/m (positive towards east) and a south-north component of -1mV/m (positive towards north) have been adopted. Since the neutral wind and the electric field used in the computations of Fig. 4 are characteristic for summer conditions under low solar activity, it is reasonable to assume that the velocity profiles of Figs 3 and 4 are permanent features for these geophysical conditions. The summer daytime valley for low solar activity, therefore, appears as a consequence of the particular structure of the vertical ion drift.

3.3. Effect of photochemical parameters

It has been shown that photochemical equilibrium cannot explain the daytime valley in the F_1 region. Photochemical parameters such as the composition parameter p, effective dissociative recombination rate a and solar ultraviolet fluxes are, however, constrained to a narrow range of values which are now discussed.
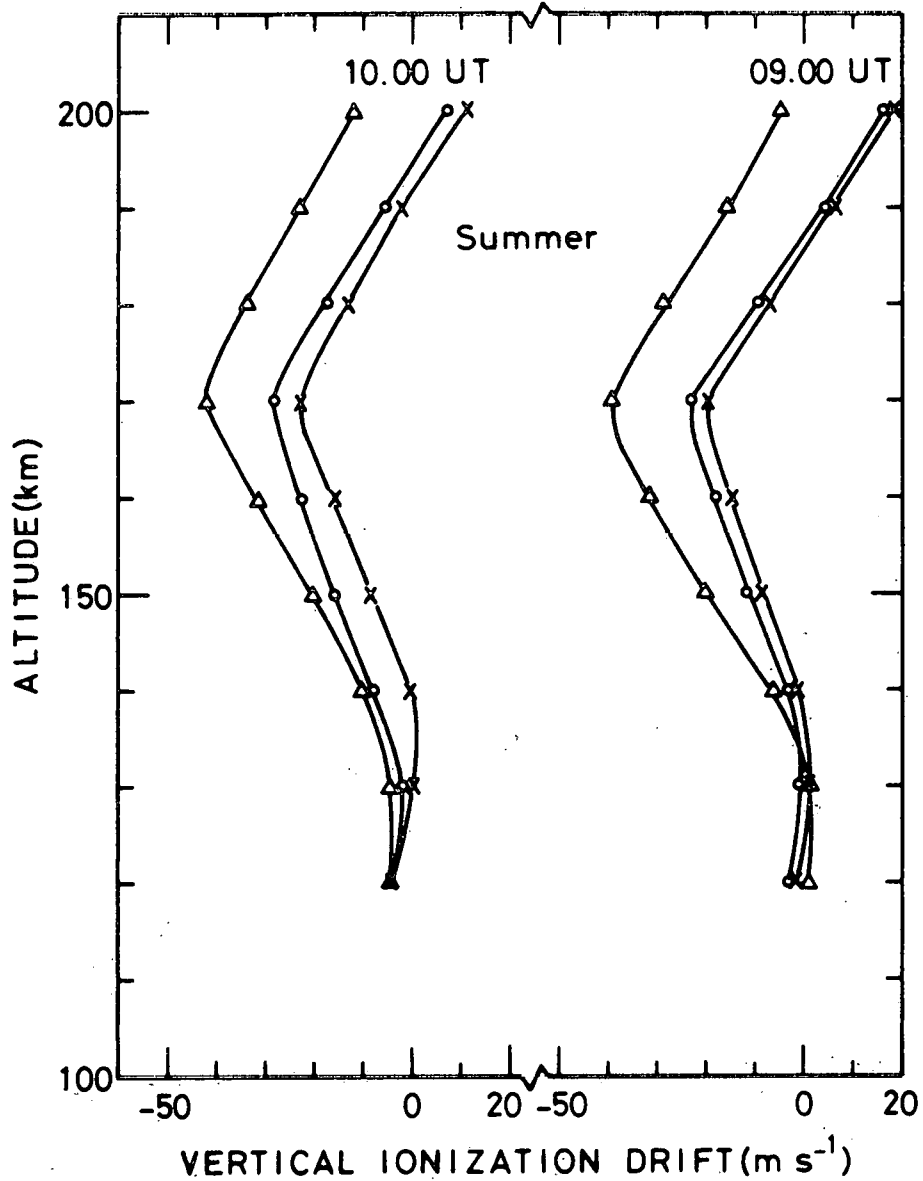
Fig. 4.- Theoretical vertical ionization drift for low solar activity summer
conditions at 09.00 and 10.00 UT. Crosses, circles and triangles respec-
tively correspond to zero electric field, to the measured electric field,
and to a predominantly east-west electric field.

A classical analysis of the equilibrium between production and loss (Rishbeth and Garriott, 1969) shows that a *ledge* can appear in the transition region where atomic ions become more abundant than molecular ions. This fact points out the necessity for a good choice of the composition parameter given by Equation (17). Using the dissociative recombination rate given by Equation (16), one obtains on Fig. 5 several electron density profiles corresponding respectively to 210, 200, 190, 180 and 170 km for the altitude parameter z_{so} where $n(O^+)/n_e = 0.5$. None of these profiles obtained without transport effect fits the observed density (dashed curve) on May 6, 1975 at 11.00 UT but, it seems that 190 km $\leqslant z_{so} \leqslant$ 200 km could represent average conditions. When the velocity profiles of Fig. 2 is introduced in the continuity equation, one obtains the results of Fig. 6 which clearly shows that $z_{so} = 190$ km is a good choice to compute the composition parameter p. Furthermore, the composition parameter directly deduced from the incoherent scatter measurements of May 6, 1975 is shown as a function of universal time on Fig. 7 for several altitudes. The composition parameters obtained with Equation (17) from Oliver (1975) are 0.31, 0.42, 0.58 and 0.79 for 165 km, 180 km, 220 km and 225 km altitude with $z_{so} = 190$ km and H = 20 km. These values used at 11.00 UT are in good agreement with the observed values of Fig. 7. An ion composition model (Torr and Harper, 1977) has been derived from Atmosphere Explorer C data for interpretation of F_1 region data at Arecibo. This model is not in contradiction with the values used in the present work.

In the previous computations the effective dissociative recombination rate was given by Equation (16). Adopting different values for a between $3.0 \times 10^{-7}(300/T_e)^{0.7}$ and 2.1×10^{-7} $(300/T_e)^{0.7}$ (cm^3 s^{-1}), one obtains the results of Fig. 8 where the transport effect previously described is taken into account. The best agreement with the observed profile results for $a = 2.3 \times 10^{-7}$ $(300/T_e)^{0.7}$ (cm^3 s^{-1}). Such a dissociative recombination rate cannot be directly compared with laboratory data (Walls and Dunn, 1974) or with *in situ* determinations (Torr *et al.*, 1977a) since the partial ion concentrations must be accurately known as can be seen from Equation (12) which defines a. The value of a falls, however, in the range of the experimental values obtained for each ion (Biondi, 1969; Walls and Dunn, 1974; Torr *et al.*, 1977a).
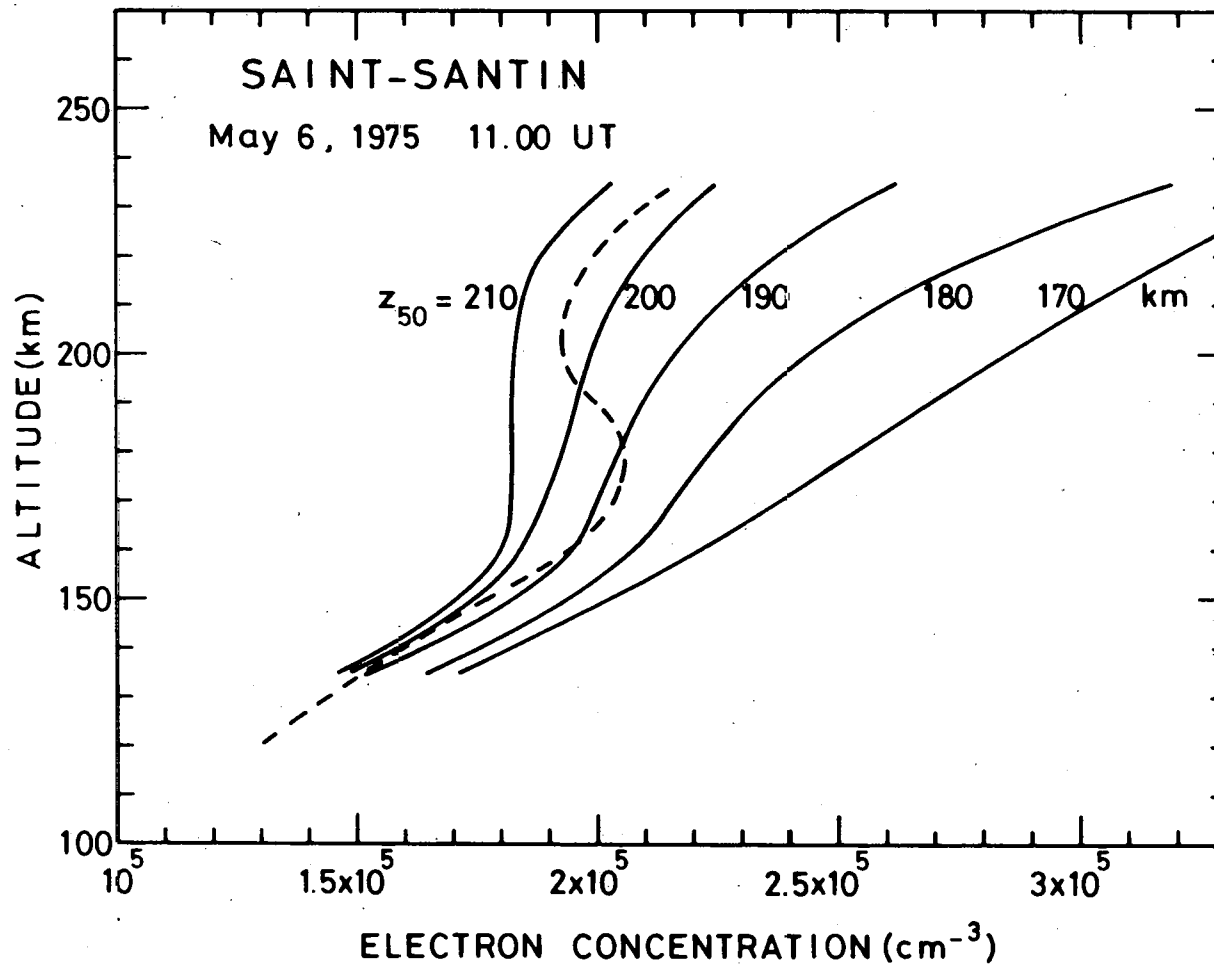
Fig. 5.- Photochemical equilibrium profiles (full curves) computed for $z_{50} = 170$ km to 210 km. Comparison with observed profile (dashed curve) at Saint-Santin on May 6, 1975 at 11.00 UT.
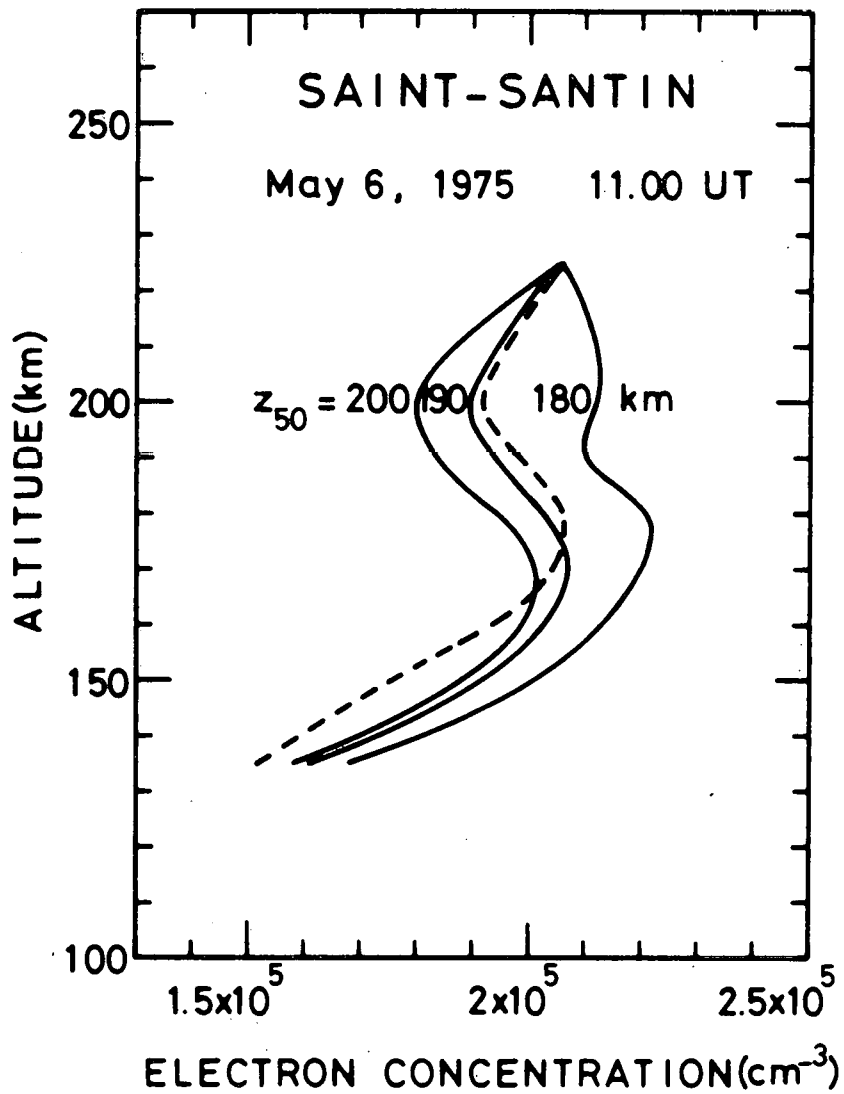
Fig. 6.- Computed profiles (full curves) obtained with the velocity model
of Fig. 2 for z_{50} = 180 km to 200 km. Comparison with observed
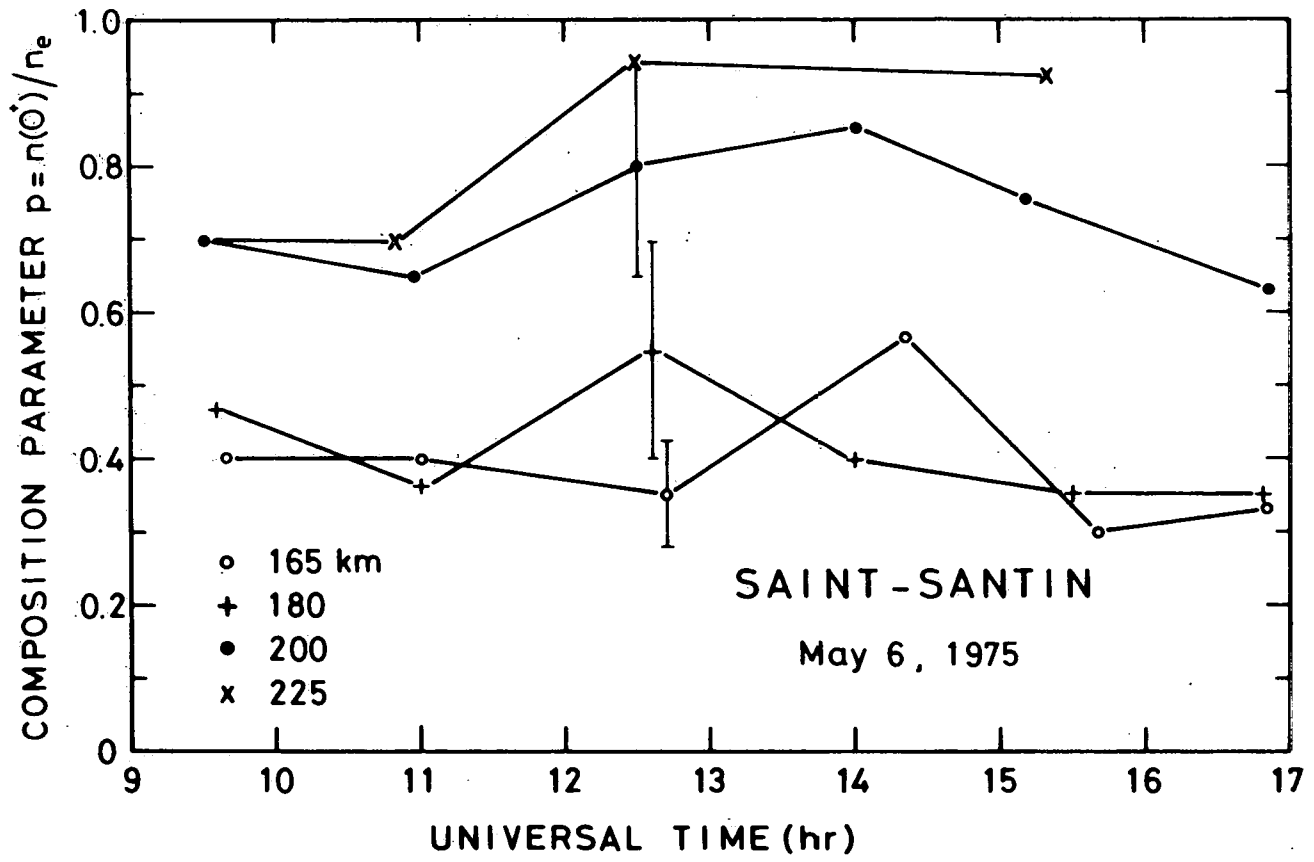(dashed curve) profile as in Fig. 5.

Fig. 7.- Experimental composition parameter p as a function of universal time for May 6, 1975 at 165 km, 180 km, 200 km and 225 km altitude.

The results presented in Figures 5, 6 and 8 are obtained with the ultraviolet fluxes (see Table I) given by Hinteregger (1976). Using the best photochemical parameters previously discussed, the same computation has been made with the solar fluxes (see Table I) obtained by Schmidtke (1976). Fig. 9 shows a comparison of electron densities obtained with Hinteregger's and Schmidtke's fluxes respectively when the upper boundary electron concentration is the observed values at 225 km in both cases. The shape of the electron distribution resulting from the use of Schmidtke's fluxes is completely different from the density computed with Hinteregger's fluxes. Such an example shows that in presence of a transport effect, the electron density in the F_1 layer is not proportional to the square root of the solar ultraviolet flux. This proportionality is, however, recovered at 140 km altitude where the vertical ion drift used in the present computations is negligible. It is furthermore interesting to note that the observed electron density of May 6, 1977 corresponds to a solar 10.7 cm radioelectric flux $F_{10.7} = 76 \times 10^{-22}$ W m^{-2} H$_z^{-1}$ whereas Hinteregger's flux measurements correspond to $F_{10.7} = 73 \times 10^{-22}$ W m^{-2} H$_z^{-1}$. Schmidtke's data were obtained for $F_{10.7} = 95 \times 10^{-22}$ W m^{-2} H$_z^{-1}$. It appears, therefore, that the differences between the two computed curves of Fig. 9 reflect a different solar activity level between May 6, 1975 and the observational conditions of Schmidtke (1976). Although there is no unique correlation between the solar decimetric flux and each individual line of the solar ultraviolet spectrum, it is clear from Fig. 9 that any attempt to fit an observed electron *daytime valley* with a theoretical model requires an accurate knowledge of solar fluxes obtained under similar conditions as the electron densities.

4. WINTER CASE WITHOUT A VALLEY

Even for low solar activity conditions, a daytime valley has never been observed above Saint-Santin (Taieb *et al.,* 1975) during winter. A typical profile of January 30, 1972 at 11.00 UT is given on Fig. 10 where the electron density rapidly increases above 160 km altitude to reach the maximum density of the F_2 peak which is located around 250 km altitude.
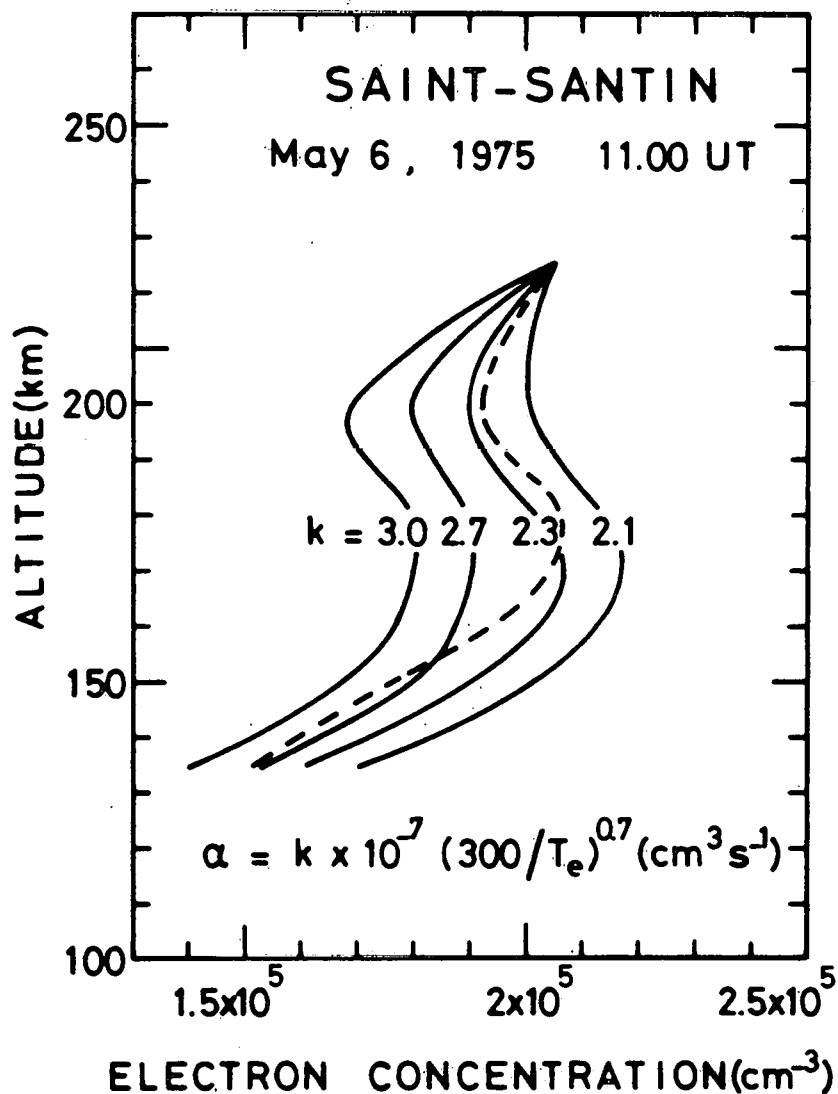
Fig. 8.- Computed profiles (full curves) obtained for different values of the effective dissociative recombination rate α. Transport effect is included. Comparison with observed profile as in Figs. 5 and 6.
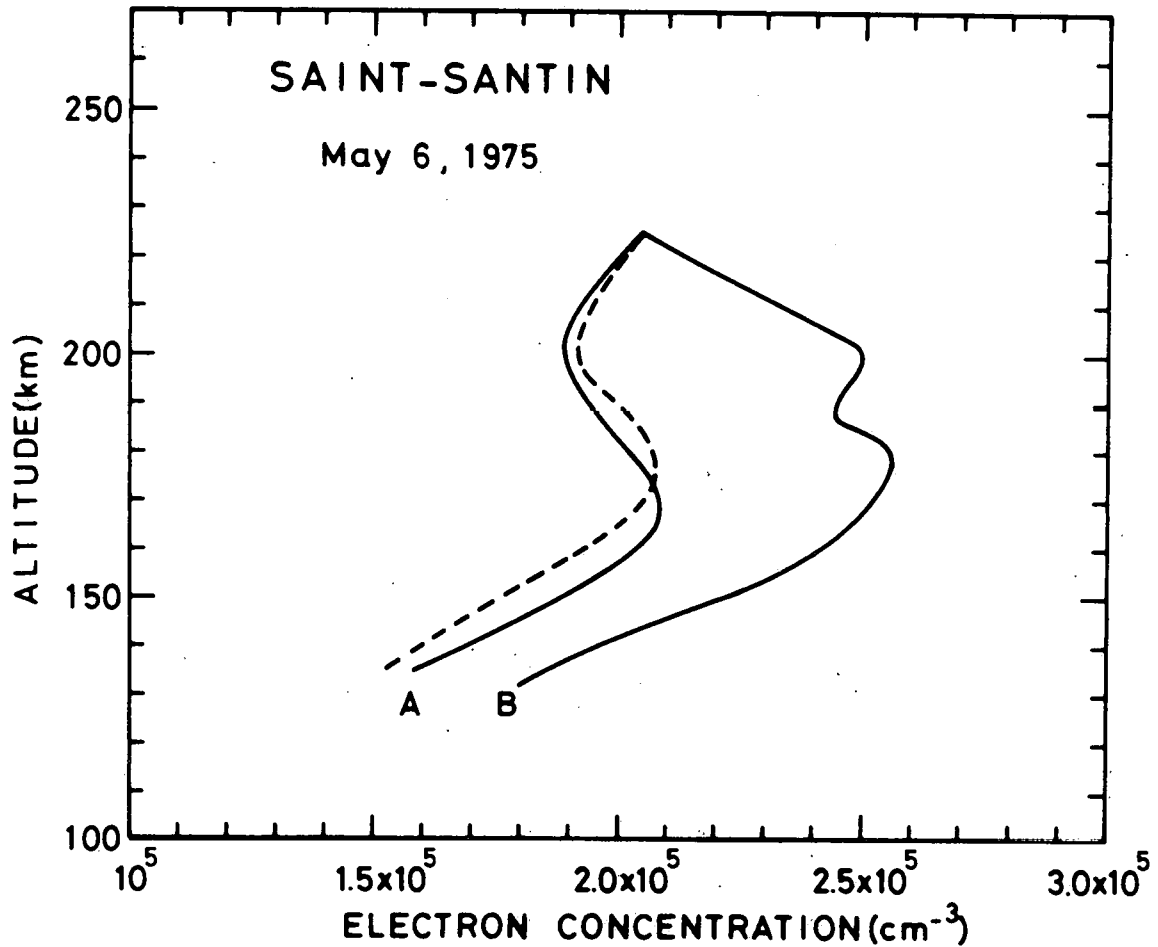
Fig. 9.- Effect of solar ultraviolet fluxes on the electron density when the transport effect is included. May 6, 1975 profile (dashed curve) corresponds to $F_{10.7} = 76 \times 10^{-22}$ Wm^{-2} Hz^{-1}. Curve A is computed with ultraviolet fluxes of Hinteregger (1976) ($F_{10.7} = 73 \times 10^{-22}$ Wm^{-2} Hz^{-1}) and curve B is computed with fluxes measured by Schmidtke (1976) ($F_{10.7} = 95 \times 10^{-22}$ Wm^{-2} Hz^{-1}).
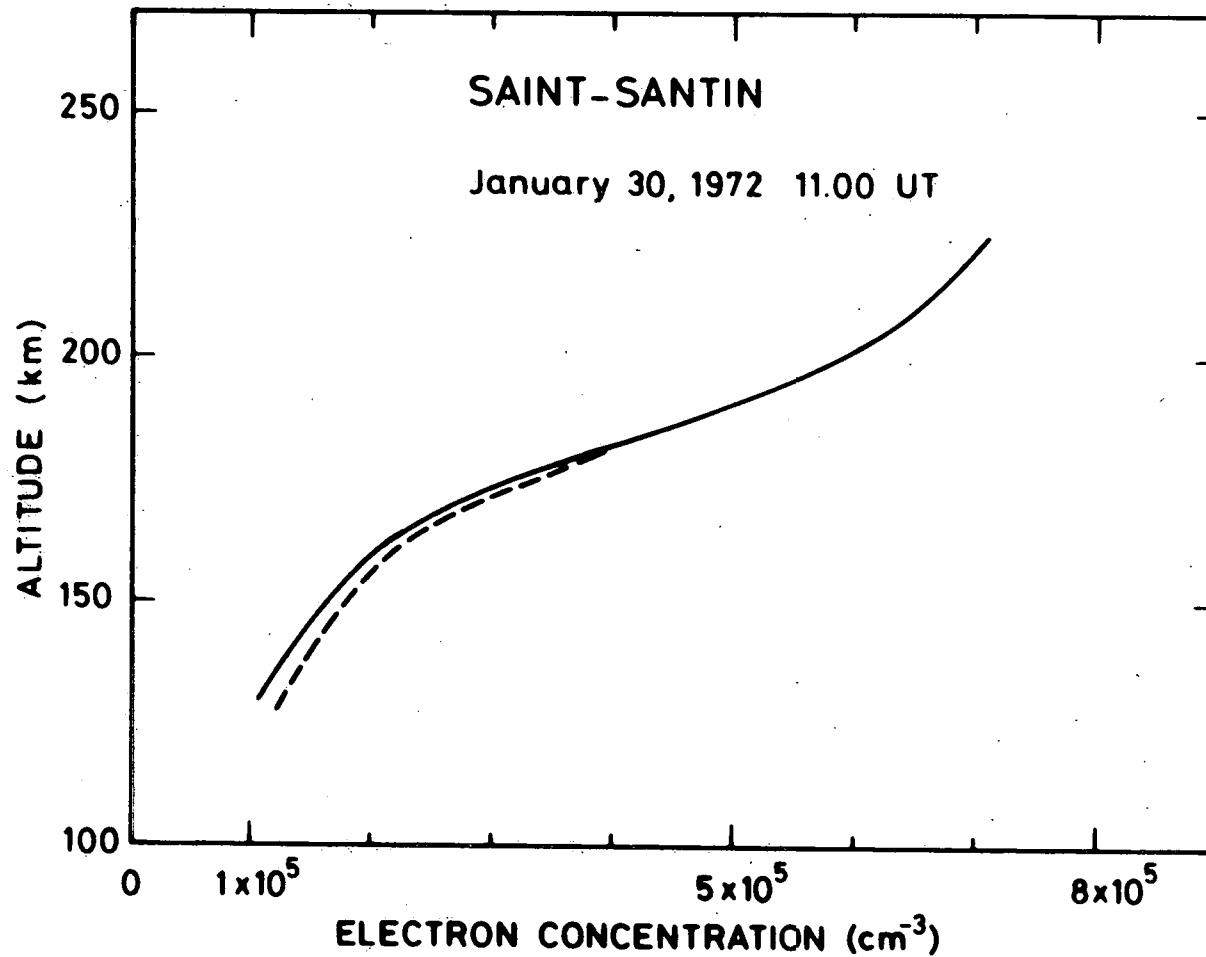
Fig. 10. Observed electron density (dashed curve) above Saint-Santin on January 30, 1972 at 11.00 UT. Comparison with computed profile (full curve).

The electron continuity equation (13) is solved with the solar fluxes of Hinteregger (1976), a solar zenith angle χ of $66.4°$ (sec $\chi = 2.50$) and an effective dissociative recombination rate given by Equation (16). The composition parameter p is computed with H = 10 km and z_{50} = 155 km. The value of z_{50} was chosen after several attempts with z_{50} ranging from 150 km to 200 km. The temperature profile is computed from Equation (1) with $T_\infty = 870$ K, $T_{120} = 335$ K and s = 0.026 km^{-1}. Neutral concentrations at 120 km altitude are taken at $45°$N for low solar activity conditions during winter (Mayr *et al.* 1976). The adopted values are n(O) = 8 x 10^{10} cm^{-3}, n(O$_2$) = 4 x 10^{10} cm^{-3} and n(N$_2$) = 2.8 x 10^{11} cm^{-3}. The ionization drift used in the computed profile of Fig. 10 is given by the full curve of Fig. 11. It appears that the vertical ionization drift for low solar activity conditions (see Fig. 11) is rather different from the summer profile of Fig. 2. As for the summer case it is interesting to compare the observed profile of Fig. 11 with a theoretical computation. Starting from Equation (18) where the various parameters are computed for winter conditions, one obtains the full curves shown on Fig. 12. These results differ from the experimental data of Fig. 11, particularly by the presence of a minimum around 180 km altitude. The full curves of Fig. 12 are, however, obtained by omitting ionic diffusion which can become important above 180 km under winter conditions as a consequence of the lowering of the F$_2$ peak in winter. The ionic diffusion velocity w_D in the F$_1$ layer can be reasonably approximated by (see Banks and Kockarts, 1973).

$$ w_D = - \frac{k T_i}{m_i \nu_{in}} \sin^2 I \left\{ \frac{m_i g}{k T_i} + \frac{1}{n_e T_i} \frac{\partial}{\partial z} \left[n_e (T_e + T_i) \right] \right\} \qquad (21) $$

where k is Boltzmann's constant, g is the acceleration of gravity, T_i and T_e are the ion and electron temperatures, m_i is the mean ionic mass, ν_{in} is the ion-neutral collision frequency, n_e is the electron concentration and I is the magnetic dip angle. The ion diffusion velocity is of the order of - 15 m s^{-1} at 200 km, - 9 m s^{-1} at 190 km, and rapidly vanishes below 180 km altitude for winter conditions. When the correction w_D given by Equation (21) is applied to the full curves of Fig. 12, one obtains the dashed curves which are in reasonable agreement with the experimental profiles of Fig. 10. The difference between summer and winter ion drift profiles essentially results from the ion diffusion which starts to become important at lower heights in the winter F$_1$ layer. Furthermore, as a consequence of the
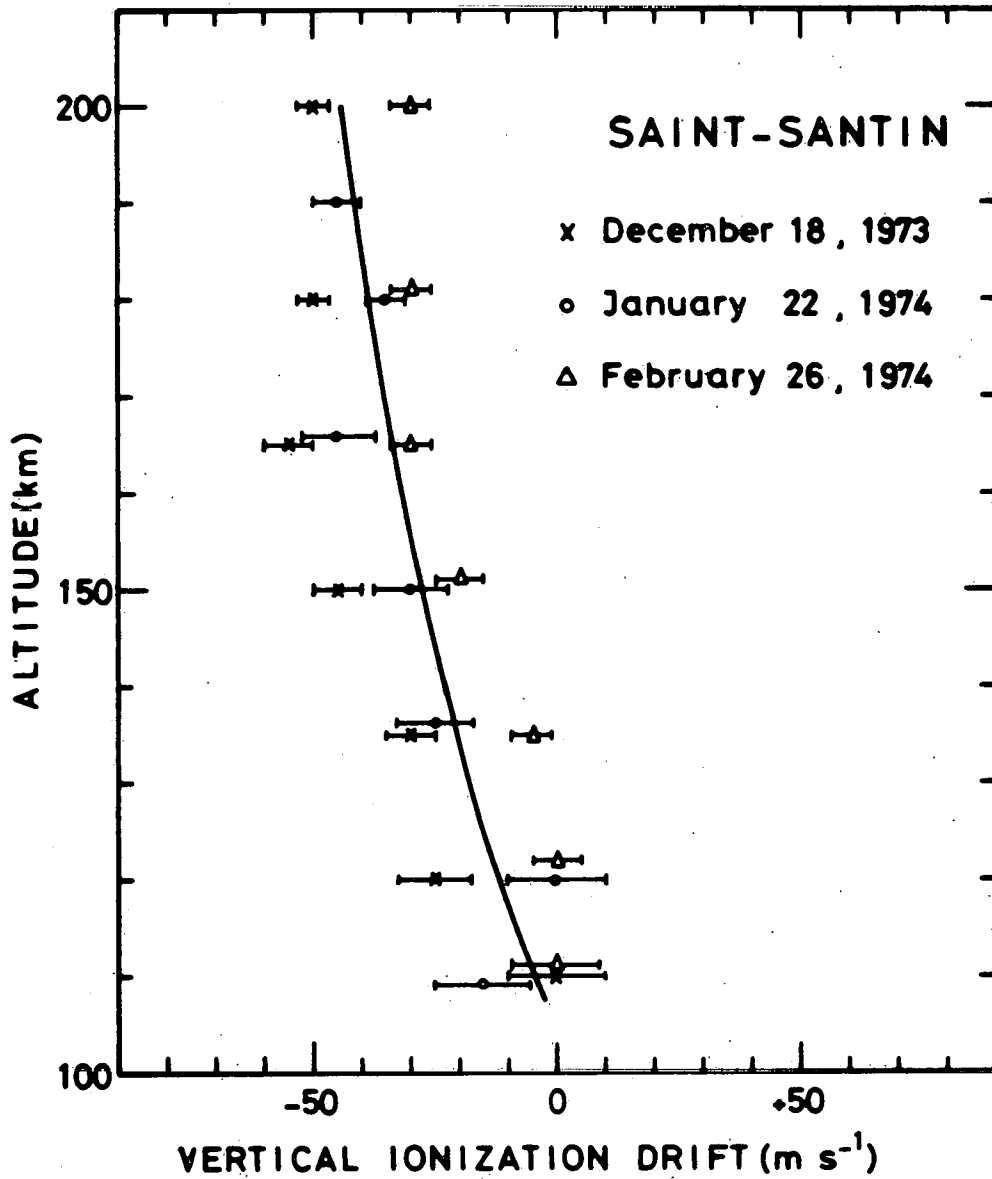
Fig. 11.- Observed vertical ionization drift above Saint-Santin on December 18, 1973 (X), January 22, 1974 (0) and February 26, 1974 (Δ). Each point corresponds to the average of measurements made between 09.30 and 13.00 UT. Full curve has been adopted for the computations.
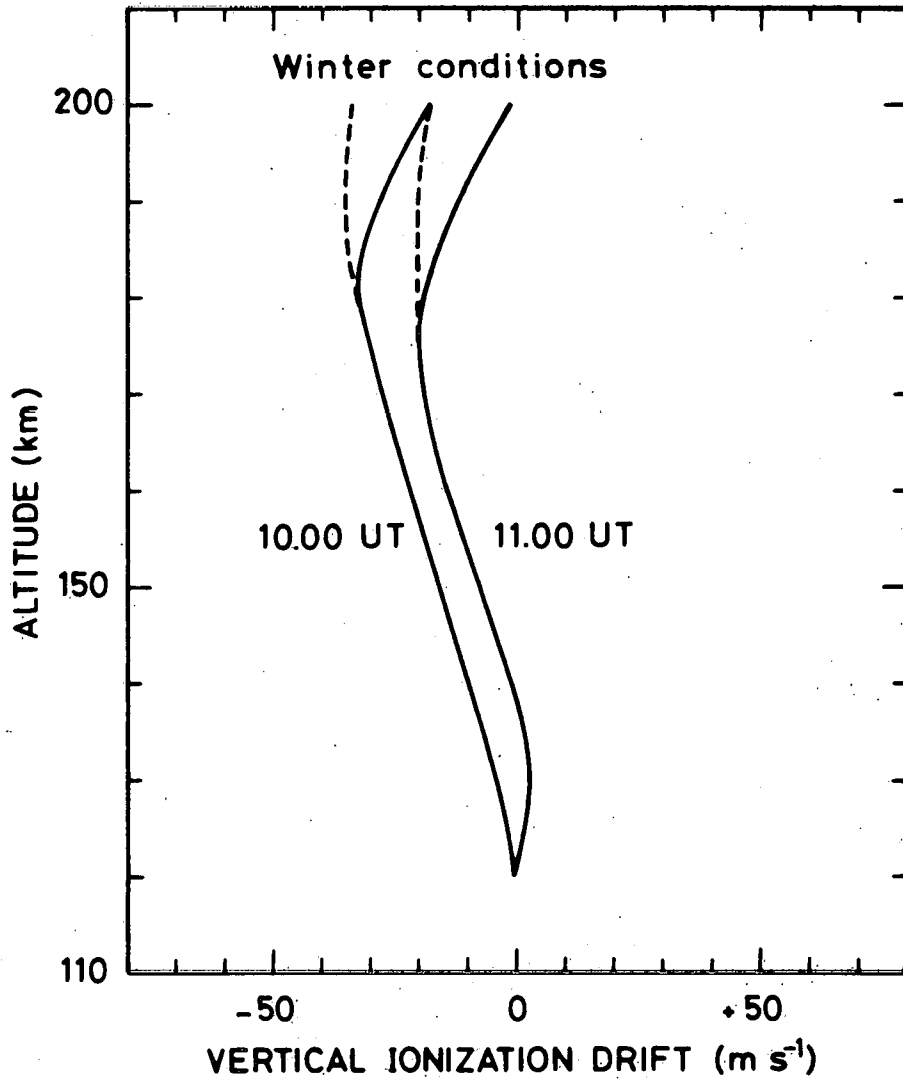
Fig. 12.- Vertical ionization drift models with (dashed curves) and without (full curves) ion diffusion transport for winter conditions.

lower altitude of the F_2 peak during winter, the vertical electron density gradient is much greater in the F_1 layer (see Fig. 10) for winter conditions. The combination of this effect and the different winter ion drift profile is responsible for the absence of a daytime valley in the F_1 layer under winter conditions.

5. CONCLUSIONS

A daytime valley has been observed in the F_1 layer above Saint-Santin during summer for low solar activity conditions. Although photochemical equilibrium theory is usually a good approximation for the ionospheric F_1 layer, it cannot explain the presence of a daytime valley even qualitatively.

The introduction of a downward vertical ionization drift in the electron continuity equation leads, however, to a satisfactory explanation. The downward drift must reach values of the order of - 25 to - 30 m s^{-1} near 180 km. Above and below this height the vertical transport tends towards zero near 130 km and 220 km altitude respectively. Such a transport, which initially was introduced to obtain an electron vertical distribution in agreement with the observations, is confirmed by measurements with the French incoherent scatter facility. The reality of the phenomenon is also emphazized by the agreement between observed and theoretical ionization drifts under low solar activity winter conditions for which the daytime valley disappears.

From the analysis of the summer daytime valley, it appears that the effective dissociative recombination rate should be $a = 2.3 \times 10^{-7} (300/T_e)^{0.7}$ (cm^3 s^{-1}), i.e. a value compatible with laboratory and in $situ$ determinations for specific molecular ions.

Furthermore, the ionizing ultraviolet fluxes must be known with great accuracy in order to explain the daytime valley. An ideal situation occurs when solar ultraviolet fluxes are measured for identical solar activity conditions as those existing at the time when the daytime valley occurs. The introduction of a transport effect destroys the proportionality

between ionizing fluxes and electron number densities.

In summary, the daytime valley in the F_1 layer above Saint-Santin is a direct consequence of a downward ionization drift characterized by maximum downward electron flux of the order of $6 - 8 \times 10^8$ electrons cm^{-2} s^{-1} around 180 km altitude.

ACKNOWLEDGMENTS

REFERENCE

AMAYENC, P., Tidal oscillations of the meridional neutral wind at midlatitude, *Radio Sci.,* 9, 281, 1974.

AMAYENC, P., Mouvements thermosphériques de grande échelle, Etude par diffusion incohérente à moyenne latitude. Thèse de doctorat d'état Université Pierre et Marie Curie, Paris 6, 1975.

APPLETON, E.V., On two methods of ionospheric investigations, *Proc. Phys. Soc.,* 45, 673, 1933.

BANKS, P.M. and KOCKARTS, G., *Aeronomy* Part A and B, Academic Press, New York, 1973.

BATES, D.R., Some problems concerning the terrestrial atmosphere above about the 100 km level, *Proc. Roy. Soc.,* 253, 451, 1959.

BAUER, P., WALDTEUFEL, P. and ALCAYDE, D., Diurnal variations of atomic oxygen density and temperature determined from incoherent scatter measurements in the ionospheric F region, *J. Geophys. Res.,* 75, 4825, 1970.

BAUER, P., WALDTEUFEL, P. and VIALLE, C., The French multistatic incoherent scatter facility, *Radio Sci.,* 9, 77, 1974.

BIONDI, M.A., Atmospheric electron-ion and ion-ion recombination processes, *Canad. J. Chem.,* 47, 1711, 1969.

BLANC, M. and AMAYENC, P., Contribution of incoherent scatter radars to the study of middle and low latitude ionospheric electric fields, pp. 61-90 in *Atmospheric Physics from Spacelab* (J.J. Burger *et al.* eds) D. Reidel, Dordrecht-Holland, 1976.

BLANC, M., AMAYENC, P., BAUER, P. and TAIEB, C., Electric field induced drifts from the French incoherent scatter facility, *J. Geophys. Res.,* 82, 87, 1977.

CARRU, H., PETIT, M., VASSEUR, G. and WALDTEUFEL, P., Résultats ionosphériques obtenus par diffusion de Thomson (1966-1967), *Ann. Géophys.,* 23 455, 1967.

HINTEREGGER, H.E., EUV fluxes in the solar spectrum below 2000 A, *J. Atmos. Terr. Phys.,* 38, 791, 1976.

LINDINGER, W., ALBRITTON, D.L., FEHSENFELD, F.C. and FERGUSON, E.E., Laboratory measurements of the ionospheric O_2^+ $(X^2\pi_g)$ and $O_2^+(a^4\pi_u)$ reactions with NO, *J. Geophys. Res.,* 80, 3725, 1975.

MAYR, H.G., BAUER, P., BRINTON, H.C., BRACE, L.H. and POTTER, W.E., Diurnal and seasonal variations in atomic and molecular oxygen inferred from Atmosphere Explorer C, *Geophys. Res. Letters*, 3 77, 1976.

OLIVER, W.L., Models of F_1 region ion composition variations, *J. Atmos. Terr. Phys.*, 37, 1965, 1975.

RISHBETH, H. and GARRIOTT, O.K., *Introduction to ionospheric physics*, Academic Press, New York, 1969.

SCHMIDTKE, G., EUV indices for solar-terrestrial relations, *Geophys. Res. Letters*, 3, 573, 1976.

SCHUNK, R.W. and WALKER, J.C.G., Theoretical ion densities in the lower ionosphere, *Planet. Space Sci.*, 21, 1875, 1973.

STUBBE, P., Frictional forces and collision frequencies between moving ion and neutral gases, *J. Atmos. Terr. Phys.*, 30, 1965, 1968.

TAIEB, C., SCIALOM, G. and KOCKARTS, G., Daytime valley in the F_1-region observed by incoherent scatter, *Planet. Space Sci.*, 23, 523, 1975.

TORR, M.R. and HARPER, R., Satellite measurements of ionic concentrations applied to low altitude incoherent scatter interpretations, *Radio Science*, 12, 461, 1977.

TORR, M.R., St-MAURICE, J.P. and TORR, D.G., The rate coefficient for the $O^+ + N_2$ reaction in the ionosphere, *J. Geophys. Res.*, 82, 3287, 1977a.

TORR, D.G., ORSINI, N., TORR, M.R., HANSON, W.B., HOFFMAN, J.H. and WALKER, J.C.G., Determination of the rate coefficient for the $N_2^+ + O$ reaction in the ionosphere, *J. Geophys. Res.*, 82, 1631, 1977b.

WALLS, F.L. and DUNN, G.H., Measurement of total cross sections for electron recombination with NO^+ and O_2^+ using ion storage techniques, *J. Geophys. Res.*, 79, 1911, 1974.

175 - VANCLOOSTER, R., First and second order approximation of the first adiabatic invariant for a charged particle interacting with a linearly polarized hydromagnetic plane wave, 1976.
Published in Planet. Space Sci., 25, 765-771, 1977.

176 - VERCHEVAL, J., Détermination des conditions de lancement de Spacelab en vue de rencontrer les exigences d'un projet d'expérience par spectrométrie d'absorption, 1977.
Publié dans ESA Scientific and Technical Review vol. 2, n° 1, p. 19, 1978.

177 - LEMAIRE, J., Impulsive penetration of filamentary plasma elements into the magnetospheres of the Earth and Jupiter.
Published in Planet. Space Sci., 25, 887-890, 1977.

178 - SIMON, P.C. and D. SAMAIN, Solar flux determination in the spectral range 150-210 nm, 1977.
Published in Solar Physics, 49, 33-41, 1976.

179 - SIMON, P.C., Le rayonnement ultraviolet du soleil et ses relations avec l'aéronomie, 1977.

180 - ACKERMAN, M., D. FRIMOUT and C. MULLER, Stratospheric methane-measurements and predictions, 1977.
To be published in Pure and Applied Geophysics.

181 - ACKERMAN, M., Stratospheric pollution related ultraviolet radiation phenomena, 1977.
To be published in Journal de Physique.

182 - BRASSEUR, G., Un modèle bidimensionnel du comportement de l'ozone dans la stratosphère, 1977.
Published in Planet. Space Sci., 26, 139-159, 1978.

183 - SIMON, P.C., Irradiation solar flux measurements between 120 and 400 nm. State of the art and future needs, 1977.
To be published in Planet. Space Sci.

184 - ACKERMAN, M., D. FRIMOUT and C. MULLER, Stratospheric CH_4, HCl and ClO and the chlorine-ozone cycle, 1977.
Published in Nature, 269, 226-227, 1977.

185 - BARLIER, F., C. BERGER, J.L. FALIN, G. KOCKARTS and G. THUILLIER, A thermospheric model based on satellite drag data, 1977.
Published in Annales de Géophysique, 34, 9-24, 1978.

186 - ARIJS, E,, J. INGELS and D. NEVEJANS, A balloon borne quadrupole mass spectrometer for the determination of the ionic composition of the stratosphere, 1978.

187 - BRASSEUR, G. and M. BERTIN, The action of chlorine on the ozone layer as given by a zonally averaged two-dimensional model, 1977.

188 - LEMAIRE, J., La pénétration du vent solaire dans la magnétosphère, 1978.
Sera publié dans Ciel et Terre.

189 - BURLAGA, L.F. and J. LEMAIRE, Interplanetary magnetic holes : theory, 1978.

190 - WISEMBERG, J. et N. VANLAETHEM-MEUREE, Mesures des sections efficaces d'absorption de constituants armosphériques dans l'ultraviolet : description du système expérimental, 1978.
Sera publié dans le Bulletin de l'Académie Royale de Belgique.

191 - VANLAETHEM-MEUREE, N., J. WISEMBERG et P.C. SIMON, Absorption des chlorométhanes dans l'ultraviolet : mesure des sections efficaces d'absorption en fonction de la température, 1978.
Sera publié dans le Bulletin de l'Académie Royale de Belgique.

192 - VANLAETHEM-MEUREE, N., J. WISEMBERG et P.C. SIMON, Influence de la température sur les sections efficaces d'absorption des chlorofluorométhanes dans l'ultraviolet, 1978.
Sera publié dans le Bulletin de l'Académie Royale de Belgique.

193 - LEMAIRE, J., M.J. RYCROFT and M. ROTH, Control of impulsive penetration of solar wind irregularities into the magnetosphere by the interplanetary magnetic field direction, 1978.